Decreasing intensity of open-ocean convection in the Greenland and Iceland seas

G.W.K. Moore, K. Våge, R.S. Pickart, I.A. Renfrew

1. Reanalyses data

The representation of winter (defined here as the period from 1 November to 30 April) air-sea interaction in the Greenland and Iceland Seas is based on fields from the ERA-40 Reanalysis[31] and the Interim Reanalysis from the ECMWF (ERA-I)[32]. The former covers the period from 1958-2002, while the latter covers the period from 1979-2014. The two share a common lineage, and, not surprisingly, during the period of overlap the correlation coefficient between surface meteorological fields over the Greenland and Iceland Sea gyres was greater than 0.9. For the air-sea heat fluxes, the root-mean-square errors were typically less than 10 W/m^2. To generate continuous time series that span the period from 1958 to the present, we employed a simple merging technique. The ERA-40 data was used for the period 1958-1978; the ERA-I data was used for the period from 1990 onwards; and for 1979-1989, a linear combination was used with the ERA-40 weighting decreasing from 1 to 0 over this period, and the ERA-I weighting increasing from 0 to 1. A small offset of ~5% equal to the difference in the respective means for the overlap period, was also added to the ERA-40 variables in the period 1958-1989 to minimize discontinuities.

2. Air-sea fluxes over sea ice

The transfer of heat and moisture across the air-sea interface are turbulent processes that are mediated by the presence of boundary layer eddies of various scales[33] . In simplest terms, this transfer is a function of the surface wind speed and the air-sea

temperature difference, for the sensible heat flux, and the air-sea humidity difference, for the latent heat or evaporative flux[34]. Higher wind speeds and larger air-sea temperature and humidity differences result in higher heat fluxes[33,35]. There is also typically a large gradient in these fluxes as one transitions from the ice covered regions, where the insulative properties of the ice reduce their magnitude, across the marginal ice zone to the open water[33,35,36]. As a result, the largest heat fluxes occur just downstream of the sea ice cover where the wind speeds are increased due to a reduction in the surface roughness across the marginal ice zone and where the air-sea temperature difference is largest[36,37]. Farther downstream, there is a reduction in the magnitude of the fluxes as the heating and moistening of the boundary layer acts to reduce the air-sea gradients of temperature and moisture[33].

In regions where sea ice is present, the fluxes that are archived in the ECMWF Reanalyses are a weighted sum of the respective fluxes into the atmosphere over open water and sea ice[38]. The insulative character of sea ice significantly reduces the transfer of heat between the atmosphere and ocean, and, as a result, the heat fluxes over sea ice are typically an order of magnitude smaller than the corresponding fluxes over open water[39]. Therefore to estimate the turbulent heat flux that the ocean experiences in partially ice covered regions, the following approach was used. By definition:

$$Q_{thf} = AQ_{thf}^{ice} + (1-A)Q_{thf}^{ocean},$$

$where: Q_{thf}$ is the total turbulent heat flux for that grid point as archived,

A is the sea ice concentration, and

Q_{thf}^{ocean} and Q_{thf}^{ice} are the turbulent heat fluxes over the open ocean and sea ice covered portions of the grid point.

Assuming that $Q_{thf}^{ice} \ll Q_{thf}^{ocean}$, then:

$$Q_{thf}^{ocean} \approx Q_{thf} / (1-A).$$

An estimate of the uncertainty in Q_{thf}^{ocean} was generated by perturbing A by $\pm 10\%$.

The impact that sea ice has on the downstream air-sea heat fluxes can be seen in Supplementary Figure 2 which shows the spatial correlation field of the winter mean sea ice concentration with Q_{thf}^{ocean} averaged over each of the two gyres. In both instances there is a large region of statistically significant positive correlation to the north and west of the respective convection sites, confirming the important role of upwind sea ice for air-sea interaction over these sites. Note that the magnitude of the correlation is higher for the Iceland Sea gyre (>0.6), than for the Greenland Sea gyre (>0.3); this may be the result of the higher variability in sea ice concentration (and more recent sea ice retreat) in the vicinity of the Greenland Sea gyre (Figs. 1-2) or possibly due to more complex air-sea interaction in this region.

3. Assessment of the statistical significance of trends and correlations

Time series of geophysical phenomenon are often characterized by serial auto-correlation or 'red noise'[40]. This leads to a reduction in the degrees of freedom associated with a particular time series that can have an impact on the significance of trends and correlations[41] To take this into account, the statistical significance of the trends and

correlations were assessed using a Monte-Carlo approach that generated 10,000 synthetic time series that share the same spectral characteristic as that of the underlying time series, thereby capturing any temporal autocorrelation[42,43]. The distribution of trends and/or correlations from the set of synthetic time series was then used to estimate the statistical significance of the actual result.

4. Modes of climate variability

The North Atlantic Oscillation (NAO), the difference in sea-level pressure between centers of action near Iceland and the Azores, is the leading mode of climate variability in the subpolar North Atlantic[44]. It has been argued to play a major role in modulating the intensity of oceanic convection in the Greenland Sea[45]. However, for the period of interest (1958-2014), the time series of Q_{thf}^{ocean} over both the Greenland and Iceland Seas are not significantly correlated with the winter mean NAO index[5] (-0.07 and -0.21, respectively). The relative strengths of the Icelandic Low and the Lofoten Low, a secondary regional circulation feature situated over the Norwegian Sea, has been shown to play an important role in the climate of the Nordic Seas[46]. The correlations of Q_{thf}^{ocean} with an index of the relative strength of these two circulation systems have substantially higher magnitudes for both gyres than those for the NAO (-0.24 and -0.49 respectively) and which are statistically significant at the 95th percentile confidence interval. This is consistent with previous work indicating that the relative strength of these two low-pressure systems modulates the magnitude of the air-sea fluxes over the Iceland Sea[47]. It also suggests, in agreement with previous studies[48,49], that modes of variability other than the NAO are needed to fully describe the climate in the region.

5. Oceanographic data

The geographical locations of the gyres in the Greenland and Iceland Seas were determined from the dynamic topography of the surface relative to 500 m using the NISE historical hydrographic database[50]. Broad minima reveal cyclonic gyres in the central Greenland and Iceland Seas. A closed contour of dynamic topography surrounding each minimum was chosen such that a sufficiently large number of homogeneous hydrographic profiles were contained within the region to obtain robust initial conditions for the mixed-layer model simulations. Most of the variability amongst the autumn profiles was inter-annual or spatial, which provides justification for using constant initial conditions for the mixed-layer model simulations.

6. Mixed-layer model details

The one-dimensional PWP[51] mixed-layer model has been shown to predict with skill the wintertime evolution of the mixed layer within similar cyclonic circulations[52]. To implement the model, fluxes of heat, freshwater, and momentum obtained from the ERA-I were imposed at the surface at each time step. The turbulent heat and longwave radiative fluxes provide the dominant contribution to the mixed-layer deepening[52]. The ERA-I has a well-documented ~20-30 W/m^2 bias in the longwave radiative flux at high latitudes[53,54] that was taken into account in the model's forcing. The model then adjusted the mixed-layer depth and properties until three stability criteria, involving the vertical density gradient and the bulk and gradient Richardson numbers, were satisfied. In light of the model's neglect of advection, as well as small-scale variability often present within a convective gyre, the agreement between the PWP model and the Argo floats in the

Iceland Sea for winters 2008 and 2012 is very good (Supp. Fig. 2). For these simulations the model was initialized by early November profiles from the floats in question and forced by 6-hourly atmospheric fluxes from the ERA-Interim reanalysis product.

The Greenland and Iceland Sea gyres have qualitatively different overall heat budgets. In the Greenland Sea the annual mean surface heat flux over the period 1980-2012 is large, 59W m^{-2}, while in the Iceland Sea it is very small, 10W m^{-2}. As such, lateral advection plays a more important role in the Greenland Sea gyre[55,56]. This was accounted for using the following parameterization. A continuous loss of 59W m^{-2} for the duration of one year corresponds to a temperature decrease of 0.45ºC over a 1000 m deep water column, which is a typical wintertime mixed-layer depth in the Greenland Sea based on Argo profiles made over the last decade. Assuming a constant rate of restratification throughout the year, a fixed amount of heat was added to the simulated temperature profile at each time step. This temperature increase was distributed throughout the water column such that the maximum temperature was near the surface (constant in the mixed layer, which was taken to be half of that inside the gyre), with an exponential decrease toward 1000 m. The shape closely resembles the difference between the mean temperature profiles within and just outside of the gyre (not shown). As Figure 4 demonstrates, with this approach the Greenland Sea simulations are in good agreement with the observed mixed-layer evolution as measured by Argo floats.

References

31 Uppala, S. M. *et al*. The ERA-40 re-analysis. *Quarterly Journal of the Royal Meteorological Society* **131**, 2961-3012, doi:10.1256/qj.04.176 (2005).

32 Dee, D. P. *et al*. The ERA-Interim reanalysis: configuration and performance of the data assimilation system. *Quarterly Journal of the Royal Meteorological Society* **137**, 553-597, doi:10.1002/qj.828 (2011).

33 Hein, P. F. & Brown, R. A. Observations of longitudinal roll vortices during arctic cold air outbreaks over open water. *Boundary-Layer Meteorology* **45**, 177-199, doi:10.1007/bf00120822 (1988).

34 Curry, J. A. *et al*. Seaflux. *Bulletin of the American Meteorological Society* **85**, 409-+, doi:10.1175/bams-85-3-409 (2004).

35 Renfrew, I. A. & Moore, G. W. K. An extreme cold-air outbreak over the Labrador Sea: Roll vortices and air-sea interaction. *Monthly Weather Review* **127**, 2379-2394, doi:10.1175/1520-0493(1999)127<2379:aecaoo>2.0.co;2 (1999).

36 Brummer, B. Boundary-layer modification in wintertime cold-air outbreaks from the arctic sea ice. *Boundary-Layer Meteorology* **80**, 109-125, doi:10.1007/bf00119014 (1996).

37 Petersen, G. N. & Renfrew, I. A. Aircraft-based observations of air-sea fluxes over Denmark Strait and the Irminger Sea during high wind speed conditions. *Quarterly Journal of the Royal Meteorological Society* **135**, 2030-2045, doi:10.1002/qj.355 (2009).

38 ECMWF. IFS DOCUMENTATION – Cy40r1. (2013).

39 Bourassa, M. A. *et al*. High-latitude ocean and sea ice surface fluxes: Challenges for climate research. *Bulletin of the American Meteorological Society* **94**, 403-423, doi:10.1175/bams-d-11-00244.1 (2013).

40 Gilman, D. L., Fuglister, F. J. & Mitchell, J. M. On the Power Spectrum of "Red Noise". *Journal of the Atmospheric Sciences* **20**, 182-184, doi:10.1175/1520-0469(1963)020<0182:OTPSON>2.0.CO;2 (1963).

41 Allen, M. R. & Smith, L. A. Monte Carlo SSA: Detecting irregular oscillations in the presence of colored noise. *Journal of Climate* **9**, 3373-3404 (1996).

42 Moore, G. W. K. Surface pressure record of Tibetan Plateau warming since the 1870s. *Quarterly Journal of the Royal Meteorological Society* **138**, 1999-2008, doi:10.1002/qj.1948 (2012).

43 Rudnick, D. L. & Davis, R. E. Red noise and regime shifts. *Deep-Sea Research Part I-Oceanographic Research Papers* **50**, 691-699, doi:10.1016/s0967-0637(03)00053-0 (2003).

44 Hurrell, J. W. Decadal trends in the North-Atlantic Oscillation - regional temperatures and precipitation. *Science* **269**, 676-679, doi:10.1126/science.269.5224.676 (1995).

45 Dickson, B. From the Labrador Sea to global change. *Nature* **386**, 649-650, doi:10.1038/386649a0 (1997).

46 Jahnke-Bornemann, A. & Bruemmer, B. The Iceland-Lofotes pressure difference: different states of the North Atlantic low-pressure zone. *Tellus Series a-Dynamic Meteorology and Oceanography* **61**, 466-475, doi:10.1111/j.1600-0870.2009.00401.x (2009).

47 Moore, G. W. K., Renfrew, I. A. & Pickart, R. S. Spatial distribution of air-sea heat fluxes over the sub-polar North Atlantic Ocean. *Geophysical Research Letters* **39**, doi:10.1029/2012gl053097 (2012).

48 Moore, G. W. K., Renfrew, I. A. & Pickart, R. S. Multidecadal Mobility of the North Atlantic Oscillation. *Journal of Climate* **26**, 2453-2466, doi:10.1175/jcli-d-12-00023.1 (2013).

49 Kelly, P. M., Goodess, C. M. & Cherry, B. S. G. The interpretation of the Icelandic sea ice record. *Journal of Geophysical Research-Oceans* **92**, 10835-10843, doi:10.1029/JC092iC10p10835 (1987).

50 Nilsen, J. E. Ø., Hatun, H., Mork, K. A. & Valdimarsson, H. The NISE data set., (Faroese Fisheries Laboratory, Torshavn, Faroe Islands, 2008).

51 Price, J. F., Weller, R. A. & Pinkel, R. Diurnal cycling: Observations and models of the upper ocean response to diurnal heating, cooling, and wind mixing. *Journal of Geophysical Research-Atmospheres* **91**, 8411–8427 (1986).

52 Våge, K., Pickart, R. S., Moore, G. W. K. & Ribergaard, M. H. Winter mixed-layer development in the central Irminger Sea: The effect of strong, intermittent wind events. *Journal of Physical Oceanography* **38**, 541–565 (2008).

53 Chaudhuri, A. H., Ponte, R. M. & Nguyen, A. T. A Comparison of Atmospheric Reanalysis Products for the Arctic Ocean and Implications for Uncertainties in Air-Sea Fluxes. *Journal of Climate* **27**, 5411-5421, doi:10.1175/jcli-d-13-00424.1 (2014).

54 Walsh, J. E., Chapman, W. L. & Portis, D. H. Arctic Cloud Fraction and Radiative Fluxes in Atmospheric Reanalyses. *Journal of Climate* **22**, 2316-2334, doi:10.1175/2008jcli2213.1 (2009).

55 Large, W. G., McWilliams, J. C. & Doney, S. C. Oceanic vertical mixing - a review and a model with a nonlocal boundary-layer parameterization. *Reviews of Geophysics* **32**, 363-403, doi:10.1029/94rg01872 (1994).

56 Latarius, K. & Quadfasel, D. Seasonal to inter-annual variability of temperature and salinity in the Greenland Sea Gyre: heat and freshwater budgets. *Tellus Series a-Dynamic Meteorology and Oceanography* **62**, 497-515, doi:10.1111/j.1600-0870.2010.00453.x (2010).

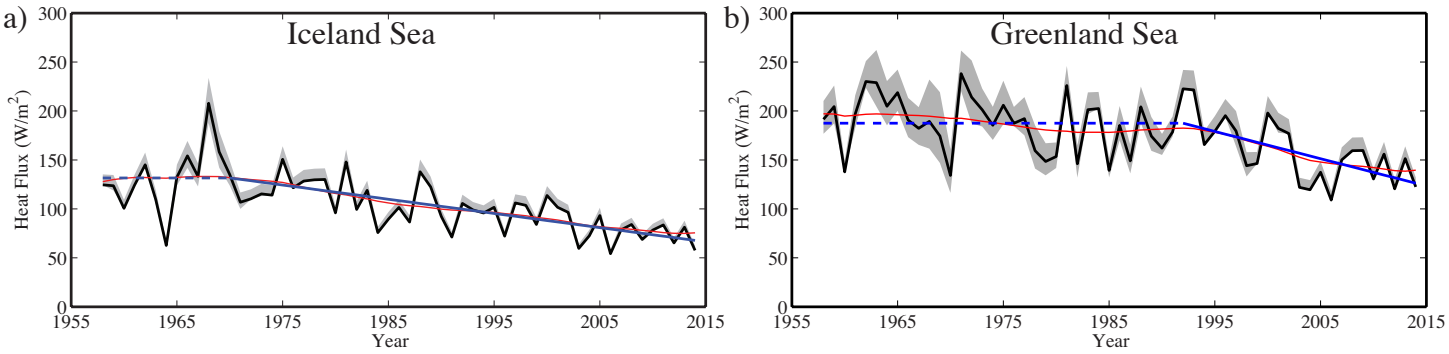

Supplementary Figure 1) Time series of the winter mean total open ocean heat flux over the Iceland and Greenland Sea gyres. Panels (a) and (b) show the open ocean total heat flux (W m^{-2}) with the shading representative of the uncertainty associated with the sea-ice concentration. The red curves are from the SSA reconstructions of the low frequency variability in the time series, while the blue lines are continuous piecewise linear least squares fits with breakpoints prescribed by the character of the respective SSA reconstructions. The trend lines that are solid are statistically significant at the 95% confidence level using a test that takes into account the reduced degrees of freedom that are the result of the autocorrelation or 'red noise' characteristic of geophysical time series. See Figure 1 for the location of the gyres.

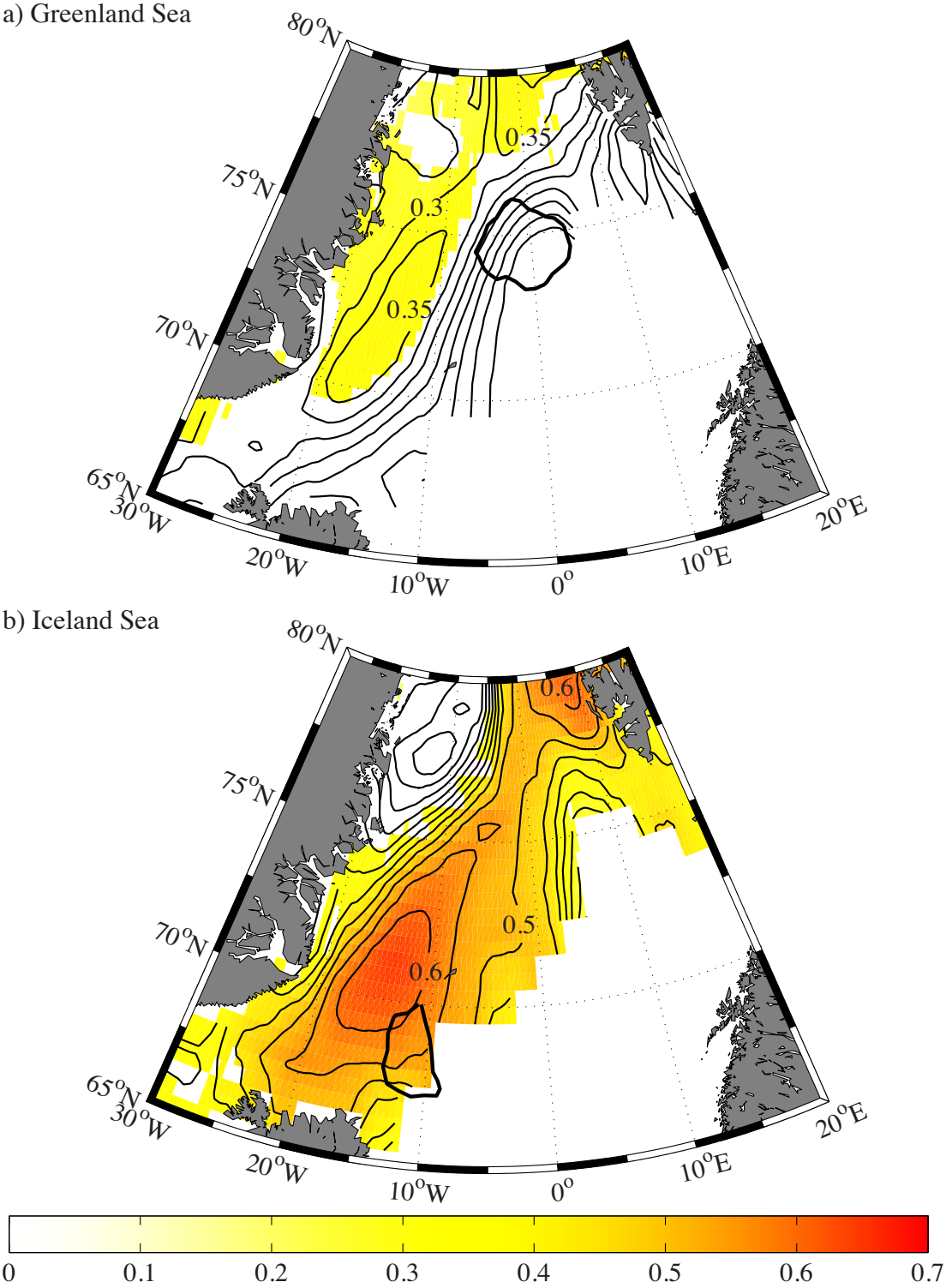

Supplementary Figure 2) Spatial correlation of the winter mean sea ice concentration field with the winter mean open ocean total heat flux over each gyre. Panels are for a) the Greenland Sea and b) the Iceland Sea. The locations of the Iceland and Greenland Sea gyres are indicated in the respective panel by the thick black curve. Shading represents the regions where the correlation is statistically significant at the 95% confidence interval.

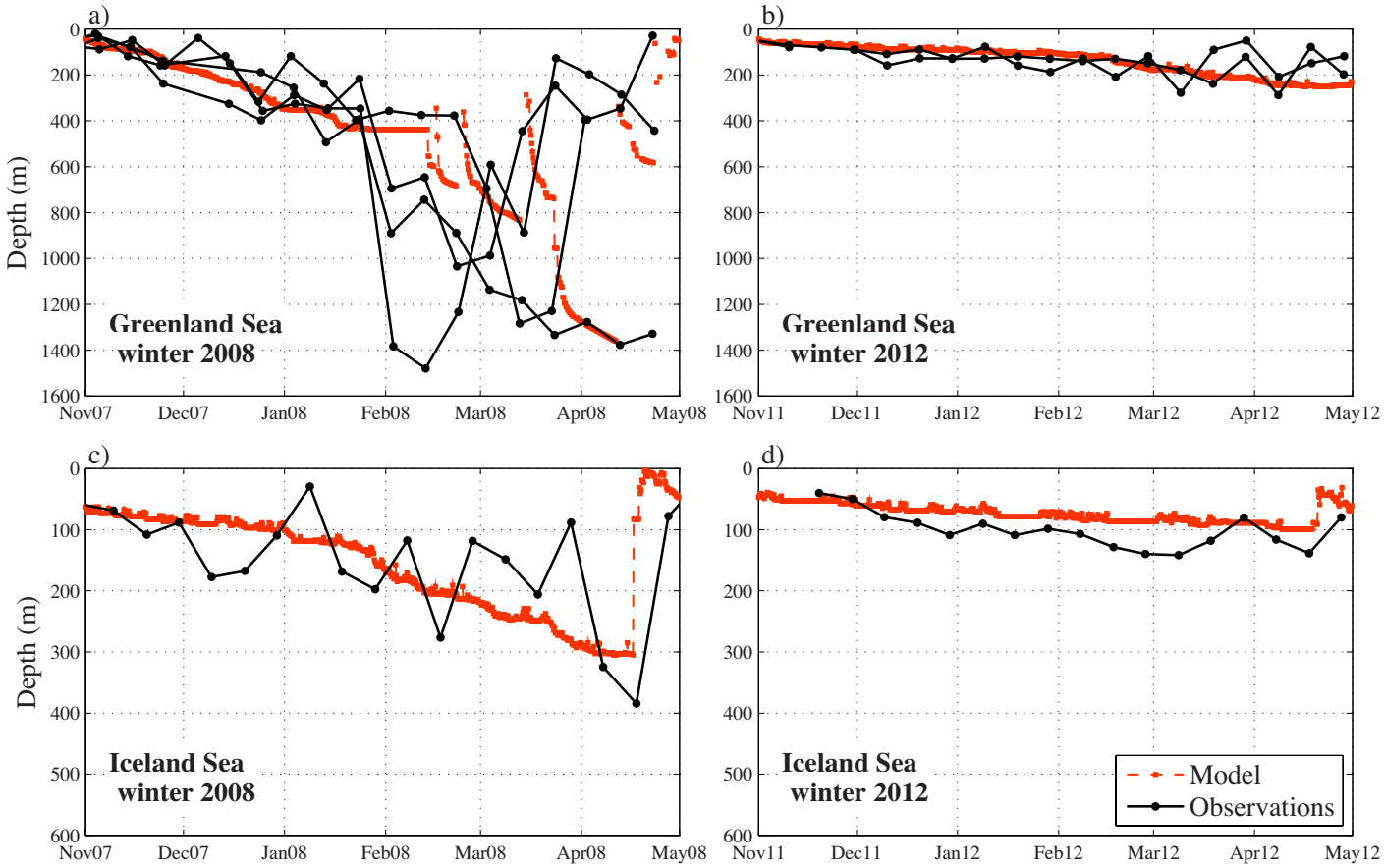

Supplementary Figure 3) Simulated and observed wintertime evolution of the mixed layers in the Greenland Sea and Iceland Sea gyres for winters 2008 and 2012. Mixed-layer depths are shown as red lines (simulated) and black crosses (observations from Argo floats). The upper row shows the Greenland Sea gyre and the lower row shows the Iceland Sea gyre. The left column is winter 2008 and the right column is winter 2012. Note the difference in vertical scale between the upper and lower rows.